Combination therapy with BPTES nanoparticles and metformin targets the metabolic heterogeneity of pancreatic cancer

Amira Elgogary[a,1], Qingguo Xu[b,c,1], Brad Poore[a], Jesse Alt[d], Sarah C. Zimmermann[d,e], Liang Zhao[f], Jie Fu[b,c], Baiwei Chen[c], Shiyu Xia[c,g], Yanfei Liu[b,c,2], Marc Neisser[c], Christopher Nguyen[a], Ramon Lee[a], Joshua K. Park[a], Juvenal Reyes[h], Thomas Hartung[f,i], Camilo Rojas[d,j], Rana Rais[d,e], Takashi Tsukamoto[d,e], Gregg L. Semenza[h,k,l,m,n,3], Justin Hanes[b,c,g,k,o,p,q,3], Barbara S. Slusher[d,e,k,r,s,3], and Anne Le[a,k,3]

[a]Department of Pathology, Johns Hopkins University School of Medicine, Baltimore, MD 21205; [b]Department of Ophthalmology, Johns Hopkins University School of Medicine, Baltimore, MD 21205; [c]Wilmer Eye Institute Center for Nanomedicine, Johns Hopkins University School of Medicine, Baltimore, MD 21205; [d]Johns Hopkins Drug Discovery, Johns Hopkins University School of Medicine, Baltimore, MD 21205; [e]Department of Neurology, Johns Hopkins University School of Medicine, Baltimore, MD 21205; [f]Department of Environmental Health Sciences, Johns Hopkins Bloomberg School of Public Health, Baltimore, MD 21205; [g]Department of Chemical and Biomolecular Engineering, Johns Hopkins University School of Engineering, Baltimore, MD 21218; [h]Department of Radiation Oncology, Johns Hopkins University School of Medicine, Baltimore, MD 21205; [i]Center for Alternatives to Animal Testing, University of Konstanz, Konstanz 78464, Germany; [j]Department of Molecular and Comparative Pathobiology, Johns Hopkins University School of Medicine, Baltimore, MD 21205; [k]Department of Oncology, Johns Hopkins University School of Medicine, Baltimore, MD 21205; [l]Department of Pediatrics, Johns Hopkins University School of Medicine, Baltimore, MD 21205; [m]Institute for Cell Engineering, Johns Hopkins University School of Medicine, Baltimore, MD 21205; [n]McKusick–Nathans Institute of Genetic Medicine, Johns Hopkins University School of Medicine, Baltimore, MD 21205; [o]Department of Biomedical Engineering, Johns Hopkins University School of Medicine, Baltimore, MD 21205; [p]Department of Neurosurgery, Johns Hopkins University School of Medicine, Baltimore, MD 21205; [q]Department of Pharmacology and Molecular Sciences, Johns Hopkins University School of Medicine, Baltimore, MD 21205; [r]Department of Medicine, Johns Hopkins University School of Medicine, Baltimore, MD 21205; and [s]Department of Psychiatry, Johns Hopkins University School of Medicine, Baltimore, MD 21205

Contributed by Gregg L. Semenza, July 12, 2016 (sent for review May 24, 2016; reviewed by Andre L. B. Ambrosio and Jacques Pouyssegur)

Targeting glutamine metabolism via pharmacological inhibition of glutaminase has been translated into clinical trials as a novel cancer therapy, but available drugs lack optimal safety and efficacy. In this study, we used a proprietary emulsification process to encapsulate bis-2-(5-phenylacetamido-1,2,4-thiadiazol-2-yl)ethyl sulfide (BPTES), a selective but relatively insoluble glutaminase inhibitor, in nanoparticles. BPTES nanoparticles demonstrated improved pharmacokinetics and efficacy compared with unencapsulated BPTES. In addition, BPTES nanoparticles had no effect on the plasma levels of liver enzymes in contrast to CB-839, a glutaminase inhibitor that is currently in clinical trials. In a mouse model using orthotopic transplantation of patient-derived pancreatic tumor tissue, BPTES nanoparticle monotherapy led to modest antitumor effects. Using the HypoxCR reporter in vivo, we found that glutaminase inhibition reduced tumor growth by specifically targeting proliferating cancer cells but did not affect hypoxic, noncycling cells. Metabolomics analyses revealed that surviving tumor cells following glutaminase inhibition were reliant on glycolysis and glycogen synthesis. Based on these findings, metformin was selected for combination therapy with BPTES nanoparticles, which resulted in significantly greater pancreatic tumor reduction than either treatment alone. Thus, targeting of multiple metabolic pathways, including effective inhibition of glutaminase by nanoparticle drug delivery, holds promise as a novel therapy for pancreatic cancer.

pancreatic ductal adenocarcinoma | glutaminolysis | glucose metabolism | KRAS mutation | intratumoral hypoxia

Patients with pancreatic ductal adenocarcinoma (PDAC) have among the highest fatality rates of all cancers (1). Pancreatic cancer is predicted to become the second-leading cause of cancer death in the United States by the year 2030 (2). Over 90% of PDACs display mutations in oncogenic *KRAS* (Kirsten rat sarcoma viral oncogene homolog) (3, 4), a known regulator of glutamine metabolism that can render cancer cells dependent on glutamine for survival and proliferation (5, 6)—a state known as "glutamine addiction" (7, 8)—suggesting that dependency on glutamine could be exploited to develop new therapies for *KRAS*-mutated PDAC. The first step of glutamine metabolism is the conversion of glutamine to glutamate and ammonia, which is catalyzed by glutaminase (GLS). Bis-2-(5-phenylacetamido-1,2,4-thiadiazol-2-yl)ethyl sulfide (BPTES), which is an allosteric, time-dependent (9), and specific inhibitor of GLS1, exhibits unique binding at the oligomerization interface of the glutaminase tetramer (10, 11). Although BPTES is more selective than other prototype glutaminase inhibitors, such as 6-diazo-5-oxo-L-norleucine (12) or ebselen (9), and can effectively inhibit GLS1 (13) and tumor growth (13–15), poor solubility (0.144 μg/mL) (16) has limited its clinical development. Recently, CB-839 (17) was tested in a phase I clinical trial. Abnormal liver and kidney function tests, lymphopenia, and hypoglycemia were reported (18).

Significance

There are no effective therapies currently available for advanced pancreatic cancer. We show that there are two populations of cancer cells within a pancreatic tumor that require targeting by different metabolic inhibitors for effective tumor control. Rapidly dividing cells use glutamine, and can be effectively killed by administration of a nanoparticle containing an inhibitor of glutamine metabolism. Hypoxic cells, which are slowly dividing cells, metabolize glucose and can be targeted by metformin, a drug used for the treatment of diabetes. Clinical trials are needed to determine whether combination therapy, with drugs that effectively block the metabolism of glutamine and glucose, improves the survival of patients with pancreatic cancer.

Author contributions: J.H., B.S.S., and A.L. designed research; A.E., Q.X., B.P., J.A., S.C.Z., L.Z., J.F., B.C., S.X., Y.L., M.N., C.N., R.L., J.K.P., J.R., C.R., R.R., and T.T. performed research; L.Z. and T.H. contributed new reagents/analytic tools; A.E., Q.X., B.P., J.A., S.C.Z., J.F., C.N., R.L., J.K.P., C.R., R.R., T.T., G.L.S., J.H., B.S.S., and A.L. analyzed data; and A.E., Q.X., B.P., J.A., S.C.Z., C.N., T.H., T.T., G.L.S., J.H., B.S.S., and A.L. wrote the paper.

Reviewers: A.L.B.A., Centro Nacional de Pesquisa em Energia e Materiais; and J.P., University of Nice.

The authors declare no conflict of interest.

Freely available online through the PNAS open access option.

[1]A.E. and Q.X. contributed equally to this work.

[2]Present address: Department of Pharmaceutical Engineering, Central South University, Changsha, Hunan 410083, People's Republic of China.

[3]To whom correspondence may be addressed. Email: gsemenza@jhmi.edu, hanes@jhmi.edu, bslusher@jhmi.edu, or annele@jhmi.edu.

This article contains supporting information online at www.pnas.org/lookup/suppl/doi:10.1073/pnas.1611406113/-/DCSupplemental.

The suboptimal chemical properties of BPTES and the clinical outcomes observed with CB-839 to date prompted us to explore alternative drug delivery strategies for glutaminase inhibitors. Using a proprietary and scalable emulsification method that creates an exceptionally dense poly(ethylene glycol) (PEG) surface layer (19), BPTES was encapsulated at high drug content into biodegradable nanoparticles (BPTES-NPs) composed of block copolymers of poly(lactic-coglycolic acid) (PLGA) and PEG. The dense PEG coating is critical to improving nanoparticle circulation time in the blood (20) and nanoparticle uptake into tumors through the enhanced permeation and retention (EPR) effect. In our present studies, nanoparticle delivery not only overcame the solubility issues associated with BPTES but also improved drug delivery to the pancreatic tumor and enhanced tumor growth inhibition. Although the efficacy of BPTES-NPs in mice was found to be similar to CB-839, BPTES-NPs were better-tolerated, showing no liver toxicity, in contrast to CB-839–treated mice. In vivo imaging using the HypoxCR reporter (21) revealed that BPTES-NPs targeted the replicating tumor cell subpopulation without affecting hypoxic cells. Using NMR and liquid chromatography-mass spectrometry (LC-MS), we found that the residual tumor cells after BPTES-NP treatment were reliant on glycolysis and glycogen synthesis. The combination of BPTES-NPs and metformin, a dual glycolysis and glycogenesis inhibitor, resulted in greater tumor reduction compared with either treatment alone.

Results

Proliferation of KRAS-Mutant Human PDAC Cells Is Dependent on Glutamine. Analysis of eight patient-derived PDAC cell lines revealed that they were dependent on glutamine for proliferation despite being grown in a glucose-rich medium (Fig. 1). PDAC cell proliferation was also sensitive to treatment with 10 μM BPTES (Fig. S1). Moreover, in the presence of glutamate, PDAC cell proliferation was significantly increased, even in the absence of glutamine or presence of BPTES (Fig. S2 *A* and *B*), providing further evidence that PDAC cell proliferation is dependent on glutamine metabolism.

Enhanced BPTES-NP Drug Exposure in PDAC Patient-Derived Tumor Orthografts. Using a unique emulsification process, which uses sucrose esters as nanoemulsion stabilizers to achieve high PEG density on the nanoparticle surface (19), we successfully encapsulated BPTES in sub–100-nm nanoparticles. BPTES-NPs possessed a spherical shape (Fig. S2*C*) with a nearly neutral surface charge (−3 mV). BPTES content in the optimized PLGA-PEG nanoparticle formulation was 22% (wt/wt) (Table S1). The nanoparticles exhibited a highly dense PEG coating, estimated to be ∼14 PEG molecules per 100 nm^2, or $[\Gamma/\Gamma^*] = 3.3$, where Γ is the actual number of PEG molecules on the nanoparticle surface per 100 nm^2 and Γ^* is the number of PEG molecules that would occupy 100 nm^2 of particle surface area if the PEG remained in an unconstrained mushroom conformation. $[\Gamma/\Gamma^*] > 1$ indicates a dense brush PEG configuration on the nanoparticle surface (22). BPTES was released at a sustained rate under infinite sink conditions in vitro (Fig. S2*D*). Sustained BPTES concentrations were found in *KRAS*-mutant patient-derived orthotopic pancreatic tumors (JH094) in mice 2 d postinjection (Fig. 2*A*), whereas unencapsulated BPTES was below the limit of quantification (<10 nM) when administered at maximum dose, which was limited by solubility and injection volume. Unencapsulated BPTES administered by intravenous (IV) route in amounts >0.1 mg in 100 μL proved to be fatal in mice. Hence, we used intraperitoneal (IP) injection of BPTES, which allowed us to achieve a maximum tolerated dose of 12.5 mg/kg. Administration of BPTES-NP enabled us to increase the amount of BPTES that could be safely injected intravenously to 1.2 mg in 100 μL or 54 mg/kg.

To further assess drug distribution and retention, we covalently bound Alexa Fluor 647 (AF647) dye to PLGA-PEG, followed by BPTES encapsulation and injection of the nanoparticles into mice bearing orthotopic pancreatic tumors. Tumors were harvested and observed directly under fluorescence microscopy without staining. Fluorescence derived from nanoparticles was detected by confocal microscopy up to 48 h postinjection (Fig. 2*B*, *Left*). Similar results were obtained using

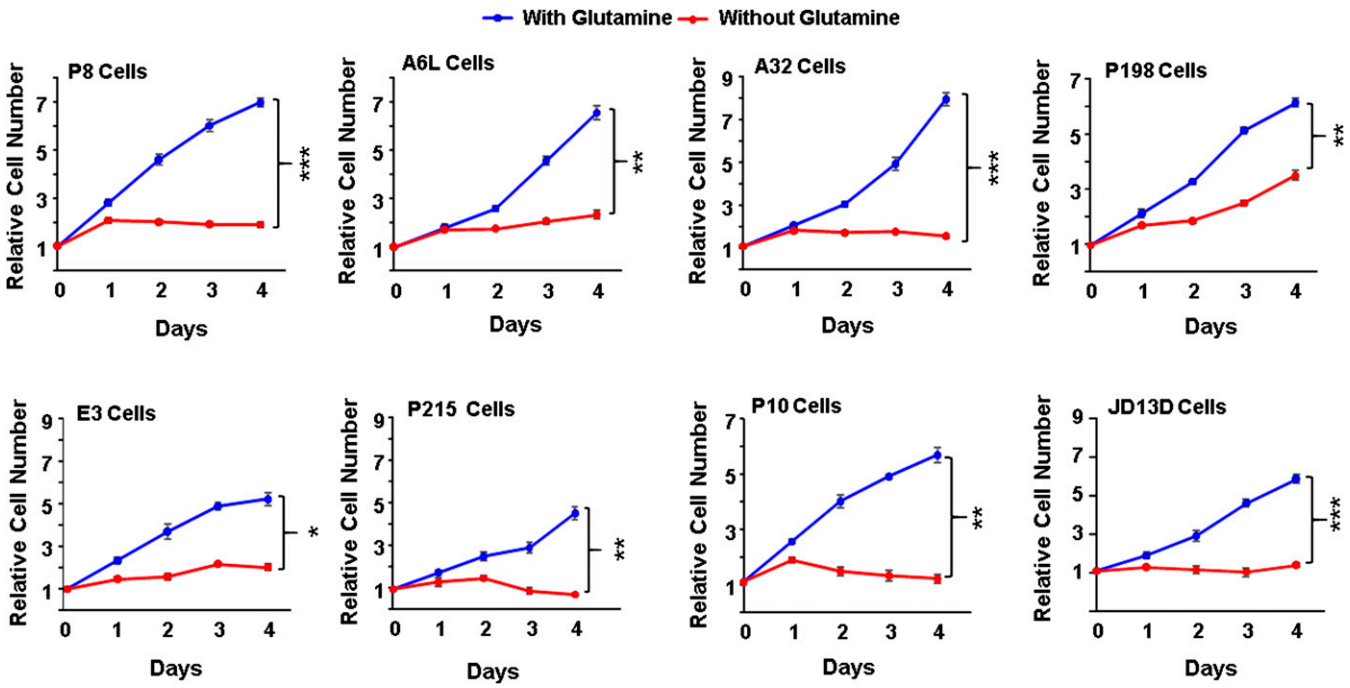

Fig. 1. Effect of glutamine deprivation on the proliferation of *KRAS*-mutated human pancreatic cancer cell lines. P8, A6L, A32, P198, E3, P215, P10, and JD13D human pancreatic cancer cells were grown at 37 °C in a 5% CO_2 and 95% air (vol/vol) incubator in 10% FBS and DMEM containing 25 mM glucose, with or without 4 mM glutamine. Data are shown as mean ± SD ($n = 4$ per time point). The entire experiment was repeated twice with similar results. $*P < 10^{-5}$, $**P < 10^{-6}$, $***P < 10^{-7}$ (Student's *t* test).

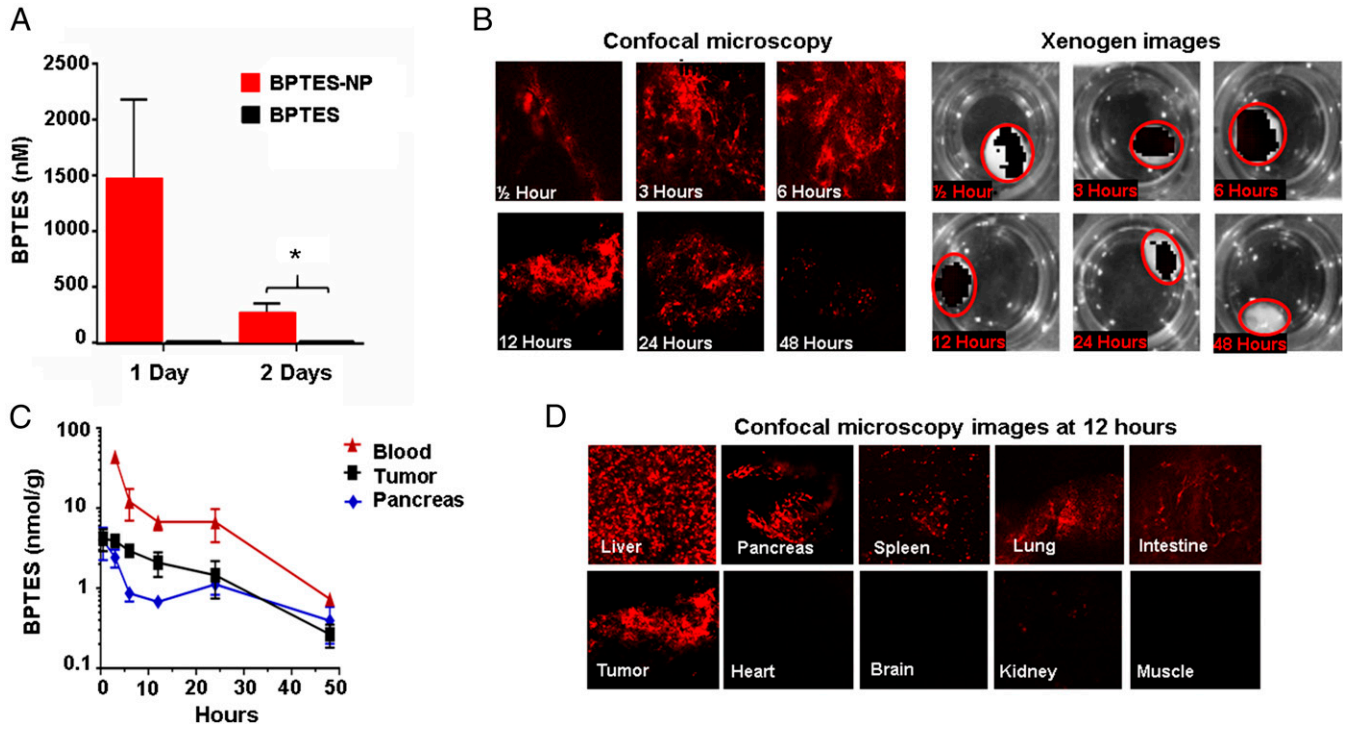

Fig. 2. BPTES-NPs delivered high drug levels to patient-derived pancreatic tumors in mice. (*A*) BPTES concentration was determined in pancreatic tumors of mice treated with BPTES-NPs (54 mg/kg i.v.) or BPTES (12.5 mg/kg, i.p.). Data are shown as mean ± SEM ($n = 8$ for day 1 and $n = 7$ for day 2). *$P < 0.01$ (Student's *t* test). (*B*) Alexa Fluor 647-labeled BPTES-NPs were observed in tumors up to 48 h postinjection by confocal microscopy (*Left*) or Xenogen imaging (*Right*; tumors circled in red) of ex vivo tumors. A 10× magnification water-dipping objective was used to acquire images. $n = 4$ per time point. (*C*) BPTES concentration was determined in blood, tumor, and normal pancreas following intravenous injection of BPTES-NPs. Data are shown as mean ± SEM ($n = 4$ per time point). (*D*) Tumor-bearing mice were injected with BPTES-NPs every 3 d via intravenous injections for a total of six injections, and tumors were harvested 12 h after the last dose for confocal microscopy. A 10× magnification water-dipping objective was used to acquire images.

Xenogen IVIS fluorescence imaging (Fig. 2*B*, *Right*). Analysis of BPTES levels in blood, tumor, and normal pancreas by LC-MS revealed measurable drug in the tumors at 48 h postinjection (Fig. 2*C*), further corroborating the confocal microscopy and IVIS imaging data. Moreover, higher concentrations of nanoparticles were found in tumors compared with other tissues, except liver (Fig. 2*D*). High-performance LC (HPLC) confirmed that the trace amount of AF647 labeling in the nanoparticles did not change the drug encapsulation efficiency (Table S1).

BPTES-NPs Attenuate Tumor Growth More Effectively than Unencapsulated BPTES. The patient-derived pancreatic orthotopic tumor model (JH094) has been shown to closely recapitulate the clinical, pathologic, genetic, and molecular aspects of PDAC (23, 24). Drug treatment was initiated after tumors reached ~50 mm^3 at 4 wk posttumor implantation. Based on the pharmacokinetic data (Fig. 2 *A*–*C*), we administered BPTES-NPs every 3 d for a total of six intravenous injections. BPTES-NPs significantly attenuated tumor growth (Fig. 3*A*). By contrast, unencapsulated

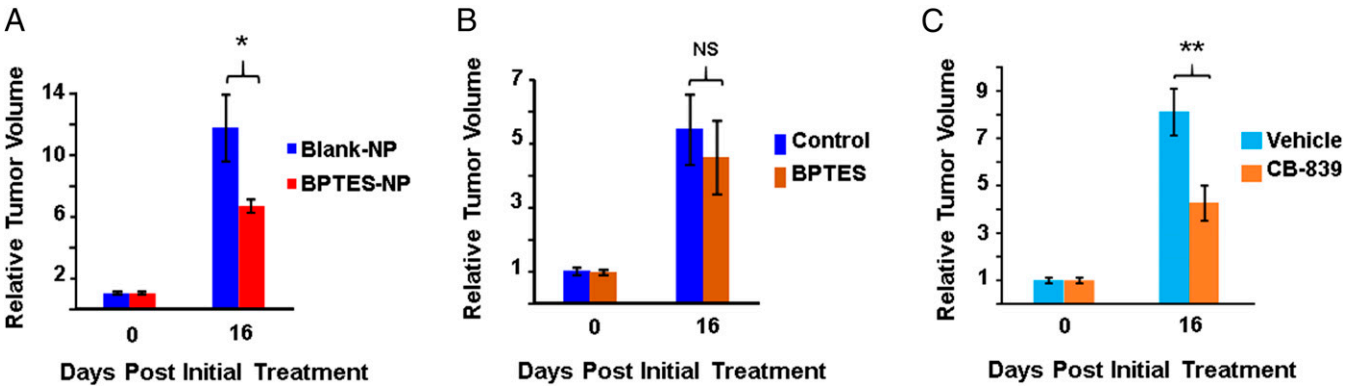

Fig. 3. Effects of BPTES-NPs, BPTES, and CB-839. (*A*) BPTES-NPs and blank-NPs were administered to tumor-bearing mice once every 3 d. Relative tumor volumes are shown as mean ± SEM ($n = 8$ per group). *$P < 0.01$ (Student's *t* test). (*B*) Tumor-bearing mice were treated with 12.5 mg/kg BPTES ($n = 12$) or vehicle control ($n = 11$). Relative tumor volumes are shown as mean ± SEM. NS, no significant difference (Student's *t* test). (*C*) The volume of patient-derived orthotopic pancreatic tumors was calculated before (day 0) and after (day 16) treatment with CB-839 (200 mg/kg, twice per day by oral gavage). Data are shown as mean ± SEM ($n = 8$ per group). **$P < 0.01$ (Student's *t* test).

BPTES exhibited no significant antitumor effect in this orthotopic model (Fig. 3*B*). Mice treated with BPTES-NPs did not lose weight or show other signs of overt toxicity. We did not find evidence of liver or kidney toxicity (Figs. S3*A* and S4*A*). Hematological studies did not show cytopenia (Fig. S4*B*) in mice treated with BPTES-NPs.

Antitumor Efficacy of BPTES-NPs Is Similar to CB-839 but Without Liver Enzyme Changes. Given that CB-839 has advanced to clinical trials, we next analyzed the efficacy of this drug versus BPTES-NPs in the same PDAC model. Using previously reported dosing information (17), we found that CB-839 required a total dose (200 mg/kg twice per d) that was >20-fold higher than that of BPTES-NPs (54 mg/kg every 3 d) to achieve comparable antitumor efficacy (Fig. 3*C*). However, unlike BPTES-NPs, CB-839–treated mice displayed elevated liver enzymes (Fig. S3*B*), which is consistent with the adverse events reported in clinical trials (18).

BPTES-NPs Selectively Target Actively Cycling Tumor Cells. We next investigated the mechanism by which glutaminase inhibition reduced tumor growth using our dual fluorescent protein reporter plasmid HypoxCR (Fig. 4*A*), which simultaneously detects hypoxic cells (hypoxia-inducible factor-dependent GFP expression) and cycling cells (G2/M/S phase-dependent mCherry expression) in vivo. This reporter has been a valuable tool for identifying and quantifying specific tumor cell subpopulations that are sensitive to drug effects (21). We transduced patient-derived PDAC cells with HypoxCR and injected these cells into mouse pancreas. At 4 wk postimplantation, BPTES-NPs were administered every 3 d for a total of six intravenous injections. Tumors were harvested for quantitative analysis by multiphoton confocal microscopy to identify subpopulations that were sensitive and resistant to BPTES-NP treatment in vivo. BPTES-NP treatment significantly diminished the mCherry-expressing population of cycling cells but had no significant effect on GFP-expressing hypoxic cells (Fig. 4 *B* and *C*). Metabolomics analysis revealed that BPTES-NP treatment significantly decreased levels of purines (guanine, adenosine) and pyrimidine precursors (uracil, aspartate, dihydroorotate) (Fig. 4*D* and Fig. S5*A*). Levels of glycine and serine, which are both used for purine synthesis, were also affected by BPTES-NP treatment (Fig. S5 *B* and *C*). Glutaminase inhibition by BPTES-NPs also increased the production of reactive oxygen species (ROS) (Fig. S5*D*), which is consistent with a previous study (14).

PDAC Cells That Survive BPTES-NP Treatment Are Reliant on Glucose Metabolism. Combination therapy with BPTES-NPs and gemcitabine, which is the current standard adjuvant chemotherapy after surgery for PDAC, using a previously reported dosing regimen for gemcitabine (25, 26), did not result in significant tumor reduction compared with treatment with gemcitabine ($P = 0.058$) or BPTES-NPs ($P = 0.46$) alone (Fig. S7*A*). To identify more effective drugs for combination treatment with BPTES-NPs, we analyzed the metabolic pathways that were active in the PDAC cells that survived glutaminase inhibition. We used NMR- and MS-based stable isotope-resolved metabolomics with [^{13}C]glucose and [^{13}C^{15}N]glutamine to follow glucose and glutamine metabolism in

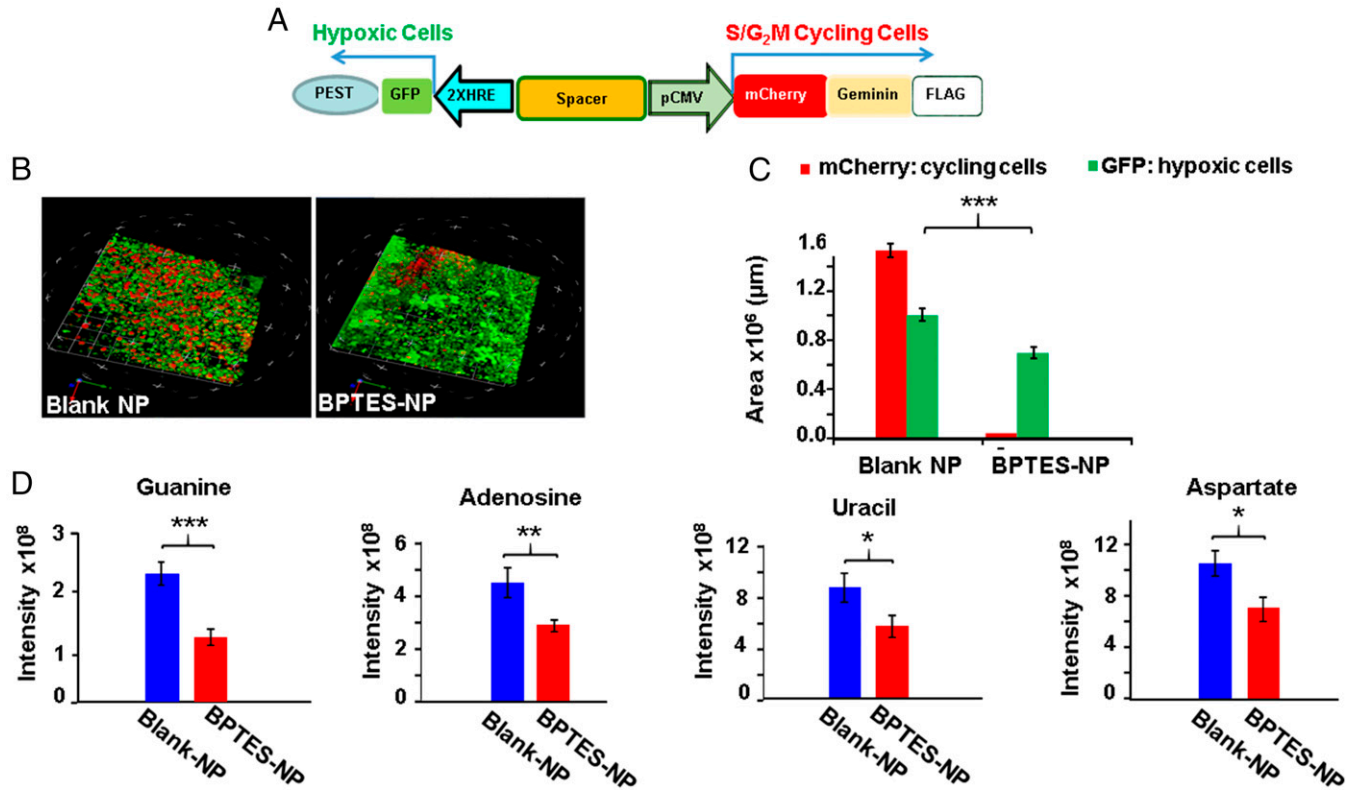

Fig. 4. BPTES-NPs selectively target the cycling tumor cell subpopulation. (*A*) Scheme of the HypoxCR dual fluorescent reporter used for detection of hypoxic and cycling cells. PEST, sequence enriched for proline, glutamate, serine, and threonine residues that decreases the half-life of GFP; 2xHRE, two copies of a hypoxia response element. (*B*) Representative confocal images taken from a total of nine tumors from mice treated with blank-NPs (*Left*) and nine tumors from mice treated with BPTES-NPs (*Right*). [Scale bars (red and green arrows), 1 μm.] (*C*) Total areas of GFP-positive and mCherry-positive cells are shown as mean ± SEM of 21 and 18 different images of tumors from mice treated with blank-NPs and BPTES-NPs, respectively. ***$P < 10^{-5}$ (Student's *t* test). (*D*) Nucleotide precursor levels in tumors from BPTES-treated and blank-NP–treated mice ($n = 8$ each) were analyzed by Q-TOF and QQQ-MS. Relative intensity (normalized by tumor wet weight) of guanine, adenosine, uracil, and aspartate peaks was determined. Data are shown as mean ± SEM. *$P < 0.05$, **$P < 0.01$, ***$P < 0.001$ (Student's *t* test).

patient-derived PDAC orthotopic tumors (27, 28). As expected, BPTES-NPs increased glutamine levels, measured either as total isotopomers detected by NMR (Fig. 5*A*) or as glutamine m+7 isotopologue detected by LC-MS (Fig. 6*A*). Because the percentage of glutamine m+7 over endogenous glutamine m+0 is less than 1% (Fig. 6*B*), BPTES-NP treatment predominantly decreased endogenous glutamate m+0 (Fig. 6*C*). We observed that [^{13}C]glucose, measured as total isotopomers detected by NMR, was avidly consumed by tumors in BPTES-NP–treated mice (Fig. 5*B*) and converted into lactate, measured as total isotopomers detected by NMR (Fig. 5*C*), leading to a significantly higher lactate:glucose ratio compared with controls (Fig. 5*D*). In addition, LC-MS showed that ^{13}C incorporation from [^{13}C]glucose into glucose-6-phosphate m+6 isotopologue (Fig. 6*D*), glucose-1-phosphate m+6 isotopologue (Fig. 6*E*), UDP-glucose m+6 isotopologue (Fig. 6*F*), and glycogen, as measured by NMR (Fig. 6*G*), was consistently enhanced in tumors from BPTES-NP–treated compared with blank-NP–treated mice. Glycogen synthesis was also found to promote cancer cell survival in hypoxia (29). The finding of these specific isotopologues suggests that increased glycogen synthesis after BPTES-NP treatment involved metabolism of glucose to glucose-6-phosphate and then glucose-1-phosphate rather than through generation of glucose-6-phosphate by gluconeogenesis (Fig. S6).

Combined BPTES-NP and Metformin Treatment Provides Enhanced Efficacy. On the basis of these metabolic findings, we analyzed the effect of metformin, a mitochondrial complex I inhibitor (30, 31) that could target hypoxic areas revealed by glycogen synthesis. Using a previously reported dosing regimen for metformin (250 mg/kg) (32, 33), we found that metformin treatment of PDAC orthotopic tumors decreased levels of lactate (Fig. 7*A*), glucose-6-phosphate (Fig. 7*B*), glucose-1-phosphate (Fig. 7*C*), and UDP-glucose (Fig. 7*D*). Combination therapy also resulted in significantly greater tumor growth inhibition compared with monotherapy with either BPTES-NPs or metformin (Fig. 7 *E* and *F*). Moreover, using patient-derived PDAC cells transfected with HypoxCR as described above, we found that metformin specifically reduced the hypoxic cell population, which was resistant to BPTES-NPs (Fig. S7*B*). Mice treated with the combination of BPTES-NPs and metformin did not lose weight or show signs of liver (Fig. S8*A*) or kidney (Fig. S8*B*) toxicity. Taken together, these results indicate that targeting by metformin of metabolic pathways used by PDAC cells that survive BPTES-NP treatment resulted in improved tumor control.

Discussion

BPTES, a prototype inhibitor, has played a critical role in establishing the potential therapeutic utility of GLS inhibition. However, poor aqueous solubility and an unfavorable pharmacokinetic profile have limited its clinical development. We created BPTES-loaded sub–100-nm PLGA-PEG nanoparticles with dense PEG coating using a proprietary nanoemulsification method (19). Encapsulation of BPTES improved its solubility, enhanced tumor targeting via the EPR effect, and increased tumor drug exposure. Nanoencapsulation allowed the safe administration of a BPTES dose that was five times greater than the maximum tolerated dose of unencapsulated BPTES. Elevated drug concentrations in the tumor, combined with prolonged drug retention, resulted in enhanced tumor reduction.

We then compared the efficacy and toxicity of BPTES-NPs with CB-839, a GLS inhibitor currently in clinical trials (18). CB-839 has an IC_{50} that is 40 times lower than BPTES (55 nM vs. 2.4 μM, respectively) (17), yet tumor growth inhibition by BPTES-NPs and

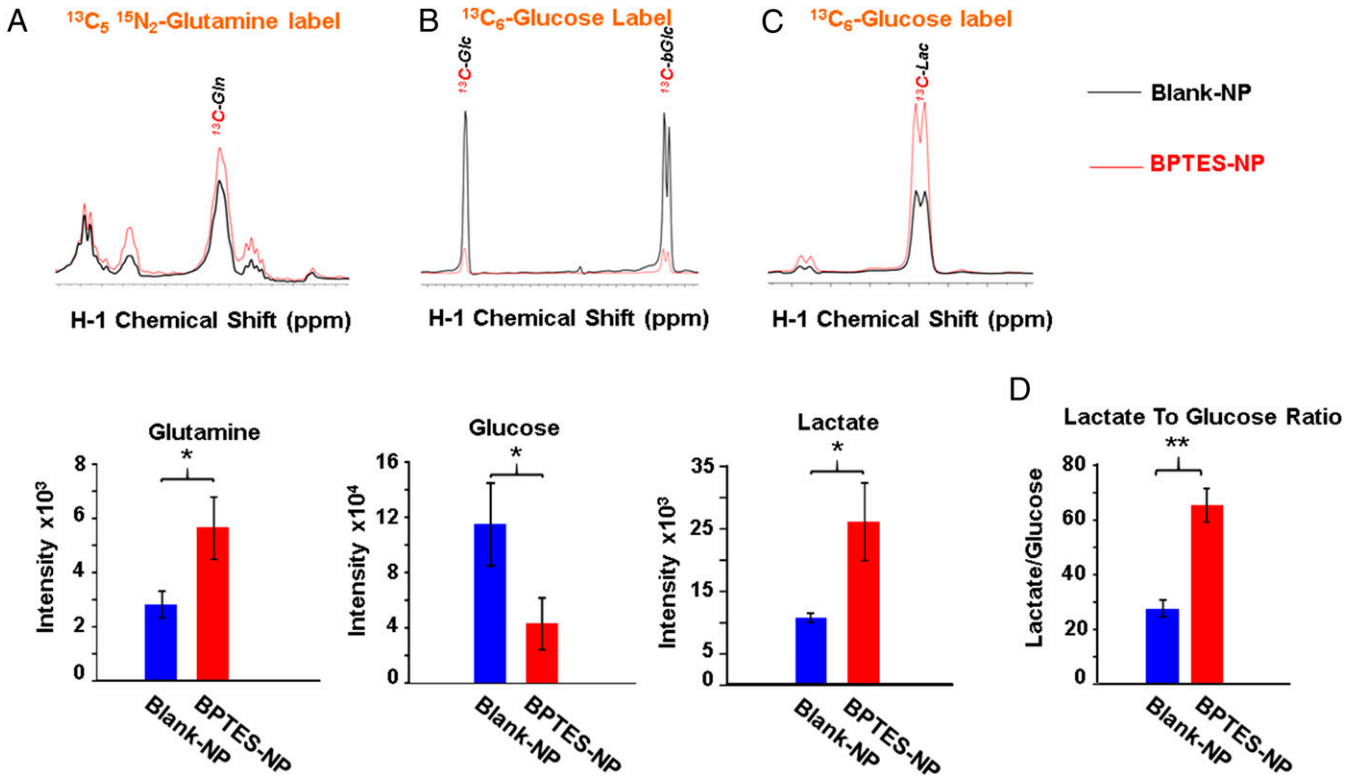

Fig. 5. Metabolomics analysis of tumors from mice treated with BPTES-NPs. (*A–C, Top*) ^{1}H^{13}C NMR spectra of ^{13}C-labeled glutamine, glucose, and lactate derived from labeled glutamine or glucose, as indicated by the orange headings. Each ^{1}H peak arose from protons directly attached to ^{13}C, and the peak assignment denotes the ^{13}C. (*A–C, Bottom*) Relative peak intensity of all isotopomers (normalized by tumor wet weight) of [^{13}C]glutamine (*A*), [^{13}C]glucose (α and β isomers) (*B*), and [^{13}C]lactate (*C*). *$P < 0.05$ (Student's *t* test). (*D*) Lactate:glucose ratio in tumors from mice treated with blank-NPs (blue bars) or BPTES-NPs (red bars). Data are shown as mean ± SEM ($n = 5$ per group). **$P < 0.01$ (Student's *t* test).

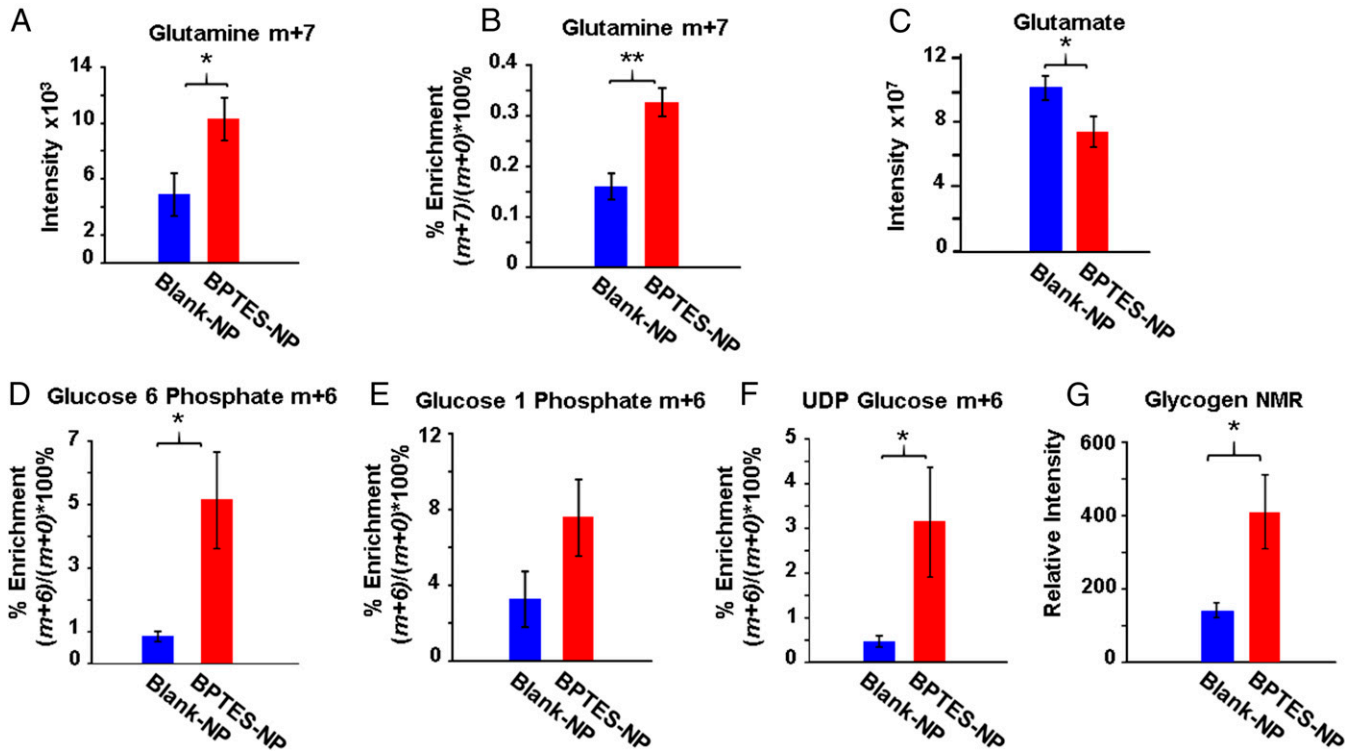

Fig. 6. Metabolites observed in residual tumors after treatment with BPTES-NPs. Mice bearing orthotopic pancreatic tumors were treated with blank-NPs or BPTES-NPs (n = 8 each) every 3 d for a total of six injections. [$^{13}C_6$]Glucose or [$^{13}C_5{}^{15}N_2$]glutamine was analyzed by NMR, Q-TOF, and QQQ-MS. (*A*) Relative intensity (normalized by tumor wet weight) of glutamine m+7 isotopologue. (*B*) Percentage of enrichment of glutamine m+7 isotopologue over glutamine m+0. (*C*) Relative intensity (normalized by tumor wet weight) of glutamate. (*D*–*G*) Relative intensity (normalized by tumor wet weight) of glucose-6-phosphate m+6 isotopologue (*D*), glucose-1-phosphate m+6 isotopologue (*E*), UDP-glucose m+6 isotopologue (*F*), and glycogen (*G*) after treatment with blank-NPs or BPTES-NPs. Data are shown as mean ± SEM (n = 8). *P < 0.05, **P < 0.01 (Student's t test).

CB-839 was similar. However, CB-839 treatment increased liver enzymes, whereas BPTES-NPs did not. PLGA and PEG are each widely used in pharmaceutical products and have a long history of safe human use (34, 35). Thus, nanoparticle encapsulation may be useful as a means to improve the pharmacokinetics and efficacy of other GLS inhibitors, including CB-839 (18), as well as newer and more potent inhibitors (36). This therapeutic strategy may be applicable to other glutamine-dependent tumors, including those with fumarate hydratase deficiency, succinate dehydrogenase deficiency, or mutant isocitrate dehydrogenase 1 or 2. It may also be effective in the treatment of patients with triple-negative breast cancer with mutation of *BRAF*, *KRAS*, or *HRAS* (37).

Treatment with CB-839 or BPTES-NPs resulted in only modest inhibition of tumor growth, indicating a resistant subpopulation of tumor cells. We hypothesized that glutaminase inhibition would affect DNA replication, because glutamine is the preferred carbon source for pyrimidine synthesis and is the nitrogen donor for N1 and N9 of purines (38). Indeed, our data showed that the cycling cell population decreased upon glutaminase inhibition. In contrast, hypoxic cells were found to be unaffected. The persistence of hypoxic cells is also consistent with previous studies, which revealed that hypoxia increases lactate production (14) and renders cells more susceptible to glycolysis inhibition (39). Metabolomics revealed active glycolysis and glycogenesis in BPTES-NP–resistant tumor cells.

Metformin is a Food and Drug Administration-approved drug used for the treatment of diabetes that inhibits glycolysis and glycogen synthesis and is currently undergoing phase III clinical trials for cancer therapy (40). We found that metformin treatment of mice bearing orthotopic PDAC tumors decreased levels of glucose metabolites involved in glycolysis and glycogen synthesis. When metformin was combined with BPTES-NPs, we observed a greater tumor reduction than with either drug alone. Previous studies reported multiple effects of metformin or phenformin on glucose metabolism (41, 42), which could contribute to the in vivo effect when combined with BPTES-NPs. These findings emphasize the need to target multiple metabolic pathways to effectively suppress PDAC growth. Metformin alone at the same dose was previously reported to have more pronounced effects on pancreatic tumor xenograft growth (43) than its effect on patient-derived orthotopic tumors in our study. Patient-derived orthotopic tumors better recapitulate the clinical, pathologic, genetic, and molecular aspects of PDAC (23, 24), including stromal content, which could affect drug sensitivity.

Glutaminase inhibitors, including BPTES, are specific to the kidney isoform GLS1 (16, 17). The majority of cancers, including PDACs, overexpress GLS1, specifically the glutaminase C splice variant (15, 44). The prevalence and importance of the kidney GLS1 isoform are well-established in various cancers (6, 15, 44), whereas GLS2 may be preferentially expressed in hypoxic PDAC cells (45) and may contribute to the ability of hypoxic cells to survive BPTES-NP treatment. We previously reported that the hypoxic cell population is sensitive to inhibition of glucose metabolism (39). The inability to target hypoxic PDAC cells with BPTES-NPs was overcome by treating the tumors with metformin.

In summary, we have shown that nanoparticle encapsulation with dense PEG surface coatings provides an effective method of delivering a GLS1 inhibitor to pancreatic tumors while minimizing toxicity. We demonstrate a selective effect of BPTES-NPs on cycling cells, whereas noncycling hypoxic cells survived BPTES-NP monotherapy. However, an increased reliance upon glucose within the surviving PDAC cells made them susceptible

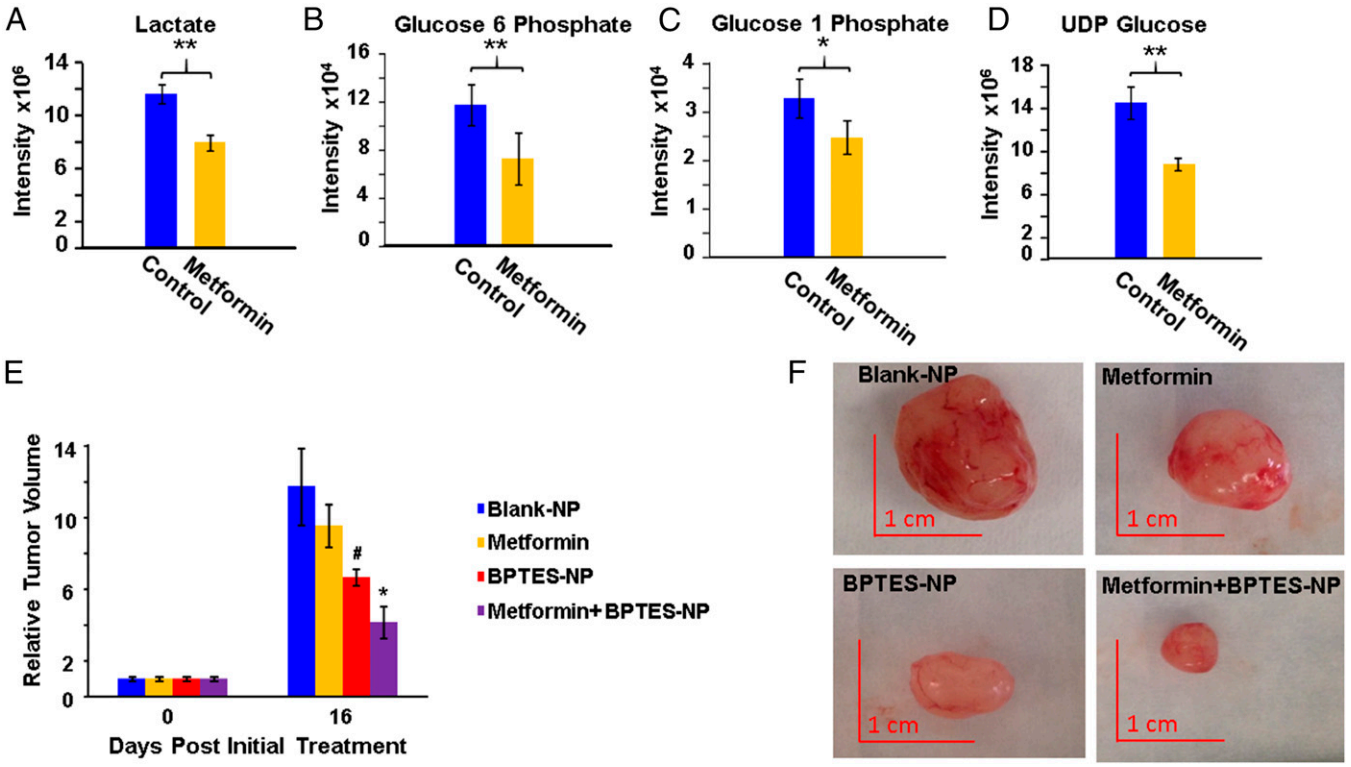

Fig. 7. (*A–D*) Metabolic effects of metformin on patient-derived orthotopic pancreatic tumors. Metformin (250 mg/kg) or vehicle was administered by daily intraperitoneal injection into tumor-bearing mice. Levels of lactate (*A*), glucose-6-phosphate (*B*), glucose-1-phosphate (*C*), and UDP-glucose (*D*) in tumors from metformin-treated and vehicle-treated mice were determined by QQQ-MS. Data are shown as mean ± SEM ($n = 8$ for vehicle and $n = 7$ for metformin). $^{*}P < 0.05$, $^{**}P < 0.01$ (Student's *t* test). (*E* and *F*) Tumor-bearing mice were treated with BPTES-NPs (54 mg/kg intravenously every 3 d) and/or metformin (250 mg/kg, i.p. every day) and tumor volumes were determined before (day 0) and after (day 16) treatment. Data are shown as mean ± SEM ($n = 7–8$). $^{*}P < 0.01$ vs. all other groups; $^{\#}P < 0.01$ vs. all other groups (Student's *t* test). Representative images of tumors from each treatment group are shown (*F*).

to metformin treatment. The ability to combat intratumoral metabolic heterogeneity with combination therapy has important implications for the design of more effective treatment strategies.

Materials and Methods

Drugs and Materials. BPTES was prepared as previously reported (16). Sugar ester D1216 was a gift from Mitsubishi-Kagaku Foods. The copolymer of PLGA (LA:GA 50:50; molecular mass 45 kDa) and PEG (molecular mass 5 kDa) was purchased from Evonik. Alexa Fluor 647 (AF647) cadaverine dye was purchased from Invitrogen. *p*-Nitrophenyl chloroformate was purchased from Sigma-Aldrich. Metformin was purchased from Santa Cruz Biotechnology. Gemcitabine was obtained through Sagent Pharmaceuticals. CB-839 was generously provided by Calithera Biosciences. All other chemicals were commercially available reagents.

Encapsulation of BPTES in Biodegradable Nanoparticles. BPTES was encapsulated into PLGA-PEG nanoparticles using small-molecular mass emulsifiers (22). Briefly, 60 mg BPTES and 300 mg PLGA-PEG were fully dissolved in 0.72 mL dimethyl sulfoxide (DMSO) and 6.78 mL dichloromethane (DCM), respectively. These two organic solutions were mixed together. One milliliter of the mixed solution containing both BPTES and PLGA-PEG was emulsified in 5 mL 1% sucrose ester D1216 solution in an ice-water bath using a probe sonicator (Vibra-Cell; Sonics & Materials) with a one-eighth inch stepped microtip under 40% amplitude for 2 min. This emulsion was poured into another 40 mL 0.5% sucrose ester solution under magnetic stirring at 700 rpm for 1 h to allow solvent to evaporate. The solvent was further evaporated by placing the suspension in a Nalgene polycarbonate desiccator under vacuum for 2 h. The final nanoparticle suspensions were centrifuged at 2,000 × *g* for 15 min, and the BPTES-NPs remaining in the supernatant were collected and washed by centrifugation at 25,000 × *g* for 25 min. Empty PLGA-PEG nanoparticles (without BPTES) were prepared using the same method, and the concentration of PLGA-PEG in DCM was 50 mg/mL.

To prepare AF647-labeled BPTES-NPs and AF647-labeled blank nanoparticles, AF647-conjugated PLGA-PEG was spiked with unlabeled PLGA-PEG in 20% weight ratio, and all other preparation steps were kept the same. Alexa Fluor 647-labeled PLGA-PEG was prepared through conjugating Alexa Fluor 647 cadaverine to *p*-nitrophenyl chloroformate–activated PLGA-PEG, as reported previously (22).

The diameter and ξ-potential (surface charge) of nanoparticles were measured using a Zetasizer Nano ZS90 (Malvern Instruments). Nanoparticle morphology was characterized using an H7600 transmission electron microscope (Hitachi). Drug content was measured by dissolving a freeze-dried BPTES-NP in acetonitrile followed by quantification by HPLC. Isocratic separation was performed on a Prominence LC system (Shimadzu) equipped with a Pursuit 5 C18 column (Varian) and a mobile phase consisting of acetonitrile/water (90/10; vol/vol) containing 0.1% trifluoroacetic acid (flow rate 1 mL/min). Column effluent was monitored by UV detection at 280 nm.

To measure the in vitro release profile of BPTES from nanoparticles, BPTES-NPs were dispersed at an original BPTES concentration of 10 μg/mL at an infinite sink condition in a PBS medium (pH 7.4) containing 0.2% Tween 80. The release solution was placed in a 1.5-mL siliconized low-retention microcentrifuge tube and incubated at 37 °C on a platform shaker at 140 rpm. At given time points, the nanoparticles were centrifuged at 25,000 × *g* for 30 min at 4 °C, and the supernatant was collected and replaced with the same volume of fresh PBS/Tween 80 solution to resuspend the nanoparticles. Supernatants (10 μL) were injected onto an Agilent 1290 UPLC system equipped with a C18 column using a gradient of 30/70 to 95/5 acetonitrile/water containing 0.1% formic acid over 1.5 min at a 0.5 mL/min flow rate. BPTES was quantified on an Agilent 6520 quadrupole–time-of-flight (Q-TOF) mass spectrometer in positive-ion mode.

Cell Culture. PDAC cells were maintained in DMEM with 10% (vol/vol) FBS and 1% penicillin/streptomycin in a 5% (vol/vol) CO_2 and 95% (vol/vol) air incubator. All cell lines (P8, A6L, A32, P198, E3, P215, P10, JD13D) were generated from PDAC tumors as previously described (46–48) and kindly provided by Anirban Maitra (MD Anderson Cancer Center, Houston). To determine glutamine dependence, cells were grown with or without glutamine in DMEM with 10% (vol/vol) dialyzed FBS and 1% penicillin/streptomycin. To determine the effect of BPTES, cells were grown in DMEM with glutamine in the presence of

10 μM BPTES in 0.1% DMSO or vehicle (0.1% DMSO). Cells were quantified using 10 μg/mL Hoechst 33342 in PBS and read by a microplate reader with excitation at 358 nm and emission at 461 nm. Viable cells were also counted once per day in a hemocytometer using trypan blue to exclude dead cells.

Patient-Derived Pancreatic Orthotopic Tumors. Animal studies were approved by the Johns Hopkins University Animal Care and Use Committee. Four-week-old female *Foxn1*^{nu} athymic nude mice (Harlan Laboratories) were maintained in accordance with the Association for Assessment and Accreditation of Laboratory Animal Care guidelines. Patient-derived pancreatic tumors were obtained from the Johns Hopkins PancXenoBank in accordance with Johns Hopkins University Institutional Review Board approval NA_00001584. Freshly resected pancreatic tumor samples obtained from patients at the time of surgery are propagated from mouse to mouse as a live tumor bank and retain their in vivo growth characteristics and defined mutation status (48). When xenograft tumors reached 50 mm^3, they were excised, cut into 1- to 2-mm^3 pieces, and dipped in Matrigel (Corning) before orthotopic implantation. A small pocket was prepared inside the pancreas into which one tumor cube was inserted and closed with an 8-0 nylon monofilament suture (49). Tumors were excised from the pancreas, weighed, and measured using digital calipers, and tumor volume (V) was calculated by the formula V = (largest tumor dimension) × (smallest tumor dimension)^2 × 0.52 (39, 49–51). Once a tumor volume of 50 mm^3 was reached (4 wk postimplantation), mice were treated with 12.5 mg/kg BPTES by intraperitoneal injection, 200 mg/kg CB-839 twice per d by oral gavage, 54 mg/kg BPTES-NPs (1.2 mg BPTES in 100 μL nanoparticles per mouse) by intravenous injection, blank-NPs (100 μL per mouse) by intravenous injection, 25 mg/kg gemcitabine intraperitoneally (25, 26), 250 mg/kg metformin intraperitoneally daily (32, 33), or a combination of BPTES-NPs with gemcitabine or metformin. BPTES-NPs were injected once every 3 d for a total of six injections over 16 d.

Reporter Gene Analysis of Pancreatic Cancer Subpopulations. The HypoxCR plasmid, psPAX2 packaging plasmid, and pMD2.G helper plasmid (Addgene) were transfected into human embryonic kidney 293T cells using Lipofectamine LTX (Life Technologies). Virus supernatants were collected every 2 d and passed through Millex syringe filter units (Millipore). Transduced cells were selected with 1 μg/mL puromycin and observed by fluorescence microscopy to detect the cycling cell subpopulation (mCherry$^+$). Cells were then exposed to 1% O_2 overnight for hypoxia assessment (GFP$^+$) after 0, 2, 4, 8, and 24 h of reoxygenation (21). To generate orthotopic tumors, 5 × 10^6 cells from each HypoxCR-pancreatic cancer cell line in 50 μL PBS and Matrigel in a 1:1 ratio were injected into the pancreas. Four weeks after implantation, mice were randomly selected for intravenous injection of BPTES-NPs or blank-NPs. Mice were treated every 3 d for a total of six injections over 16 d. Tumors were excised, bathed in PBS, and cut into slices of several millimeters in thickness and placed into a glass-bottom FluoroDish (Thermo Fisher) for imaging with an LSM 510 META multiphoton confocal microscope (Zeiss) with lasers for detection of mCherry and GFP. LSM Imagine Browser, Volocity 5 (PerkinElmer), and MetaMorph (Molecular Devices) software of the Ross Confocal Microscopy Facility were used for fluorescence quantification after image acquisition from both channels using a 10× objective and z step of 2.5 μm.

Drug Distribution and Retention in Vivo. Once a tumor volume of 50–100 mm^3 was reached, mice were injected intravenously with AF647-labeled BPTES-NPs or AF647-labeled blank-NPs. The mice were killed at 0.5, 3, 6, 12, 24, and 48 h postinjection, blood was taken via cardiac puncture, and tumors, heart, liver, lungs, thigh muscle, pancreas, spleen, kidney, brain, and intestine were removed. Organs were washed in PBS and cut into equal parts for fluorescence analysis and LC-MS to determine BPTES concentration as described below. Nanoparticle distribution images of the organs by two-photon microscopy were obtained by LSM 510 META confocal microscopy with a laser for an excitation wavelength of 651 nm and emission wavelength of 672 nm. Images were obtained with a 10× objective. Concentrations of the AF647-labeled nanoparticles in tumors were also determined by ex vivo imaging using the Xenogen IVIS spectrum optical imaging system at excitation wavelength of 640 nm and emission wavelength of 680 nm with a field of view of 12.8 cm.

Pharmacokinetics of BPTES and BPTES-NPs. Mice were treated with BPTES (12.5 mg/kg i.p.) or BPTES-NPs (54 mg/kg intravenously) and tissues were harvested as described above. To quantify BPTES, methanol containing 5 μM losartan as an internal standard was added at 5 μL/mg tissue or 5 μL/μL blood. Tissues were homogenized by mortar and pestle and sonicated on ice for 20 min. Homogenates and blood from untreated animals were spiked with BPTES from 10 to 0.003 nmol/g tissue by serial dilution to generate a standard curve. Tissue and blood homogenates were then vortexed and centrifuged at 16,000 × *g* for 5 min at 4 °C to precipitate proteins. Supernatants were transferred to 96-well plates and an aliquot (10 μL) was injected onto an Agilent 1290 UPLC system with a C18 column using a gradient of 30/70 to 95/5 acetonitrile/water containing 0.1% formic acid over 1.5 min at a 0.5 mL/min flow rate. BPTES was quantified by an Agilent 6520 Q-TOF mass spectrometer. Standards within the quantifiable range were used to generate a standard curve. The limit of quantitation was 10 nM.

Metabolite Analysis After BPTES-NP Treatment. We injected uniformly labeled [$^{13}C_5{}^{15}N_2$]glutamine or [$^{13}C_6$]glucose into mice treated with blank-NPs, BPTES-NPs, or metformin at the end of their respective treatments to follow glucose and glutamine metabolism in vivo as previously described (27, 28). Specifically, 100 μL sterile-filtered [$^{13}C_6$]glucose [20% (wt/vol)] or [$^{13}C_5{}^{15}N_2$]glutamine (100 mM) in PBS was injected intraperitoneally, three injections each 15 min apart. Tumors were harvested at 2 h post first injection and immediately snap-frozen in liquid N_2, homogenized in liquid N_2, and subjected to metabolite extraction using 1:2:0.8 chloroform:methanol:water to generate aqueous, organic, and protein fractions (52). Samples were standardized based on protein concentration and tumor wet weight. Metabolite data from these samples were acquired using an Agilent 6550 Q-TOF mass spectrometer with an Agilent 1290 HPLC. Data were analyzed using Agilent MassHunter and Agilent Qualitative and Quantitative Analysis software packages. Metabolites were identified using in-house compound standard databases with predetermined retention time and known mass-to-charge ratio. In parallel, metabolites were identified using MS/MS fragmentation data under identical conditions. In addition to Q-TOF, which is primarily used for discovery and qualitative screening experiments, we used a 6490 triple-quadrupole (QQQ) mass spectrometer to confirm the findings from discovery and qualitative screening experiments. We identified NMR peaks using Mnova software (Mestrelab Research) and our own database and normalized the peak areas to a known concentration of standard trimethylsilyl propionate. The NMR- and MS-based analysis gave an enhanced coverage of total metabolites and also cross-validated one another. ^{13}C and ^{15}N isotopomers or isotopologues were identified by NMR or LC-MS, respectively, and their fractional enrichment was quantified according to natural isotope abundance contributions to each of the isotopologues in the MS data (52–55). To establish metabolic differences between sample groups, the individual metabolites identified were compared with the raw chromatogram and peak area values using Agilent Qualitative and Quantitative Analysis software packages for each sample. Once the main discriminators were determined, their correlations in terms of metabolic pathways were established using known biochemical relationships as established in databases including KEGG (56), Reactome (57, 58), HumanCyc (59), and HMDB (60).

Drug Toxicity Assessment. At the end of each treatment, mice were killed by CO_2 asphyxiation. Cardiac puncture was performed by the Johns Hopkins Phenotyping and Pathology Core. Blood was examined for neutrophil, lymphocyte, monocyte, eosinophil, basophil, and red blood cell counts as well as hemoglobin, hematocrit, mean corpuscular volume, mean corpuscular hemoglobin, red cell distribution width, thrombocyte count, alanine aminotransferase, aspartate aminotransferase, albumin, alkaline phosphatase, gamma-glutamyl transferase, calcium, uric acid, creatinine, total bilirubin, albumin, total protein, cholesterol, high-density lipoprotein, triglycerides, glucose, and lactate dehydrogenase (39).

ROS Detection. ROS were detected using 6-carboxy-2′,7′-dichlorodihydrofluorescein diacetate (carboxy-H2DCFDA; Thermo Fisher). A concentration of 10^5 cells per milliliter was treated with blank-NPs, 10 μM BPTES-NPs, 40 mM metformin, or 40 mM metformin + 10 μM BPTES-NPs for 24 h. Fluorescence intensities of cells stained with 20 μM carboxy-H2DCFDA were recorded with excitation at 495 nm and emission at 520 nm.

Statistical Analysis. All values are reported as the mean ± SD or SEM as described in the figure legends. Significance was determined as $P < 0.05$ using Student's *t* test.

ACKNOWLEDGMENTS. We thank Dr. James Eshleman for access to the PancXenoBank, and the Ross Confocal Microscopy Facility, Wilmer Microscopy and Imaging Core Facility, and Drug Delivery and Nanotechnology Core of the Wilmer Eye Institute (NIH P30EY001765) at Johns Hopkins. Special thanks to the Institute for Clinical and Translational Research for Translational Laboratory Core support. This work was supported by NIH Grants R01-CA193895 (to A.L., B.S.S., and J.H.), R03-DA032470 (to B.S.S.), R21-CA169757 (to A.L.), P30-MH075673 (to B.S.S.), UL1 TR001079 (to B.S.S.), F32CA200275 (to S.C.Z), and R21NS074151 (to T.T.). This publication was made possible by the Johns Hopkins Institute for Clinical and Translational Research, which is funded in part by Grant UL1 TR 001079 from the National Center for Advancing Translational Sciences, a component of the NIH, and NIH Roadmap for Medical Research.

1. Hernandez BY, et al. (2010) Preview of Hawaii cancer facts and figures 2010. *Hawaii Med J* 69(9):223–224.
2. Rahib L, et al. (2014) Projecting cancer incidence and deaths to 2030: The unexpected burden of thyroid, liver, and pancreas cancers in the United States. *Cancer Res* 74(11): 2913–2921.
3. di Magliano MP, Logsdon CD (2013) Roles for KRAS in pancreatic tumor development and progression. *Gastroenterology* 144(6):1220–1229.
4. Bryant KL, Mancias JD, Kimmelman AC, Der CJ (2014) KRAS: Feeding pancreatic cancer proliferation. *Trends Biochem Sci* 39(2):91–100.
5. Birnbaum DJ, et al. (2011) Genome profiling of pancreatic adenocarcinoma. *Genes Chromosomes Cancer* 50(6):456–465.
6. Son J, et al. (2013) Glutamine supports pancreatic cancer growth through a KRAS-regulated metabolic pathway. *Nature* 496(7443):101–105.
7. Reitzer LJ, Wice BM, Kennell D (1979) Evidence that glutamine, not sugar, is the major energy source for cultured HeLa cells. *J Biol Chem* 254(8):2669–2676.
8. Wise DR, et al. (2008) Myc regulates a transcriptional program that stimulates mitochondrial glutaminolysis and leads to glutamine addiction. *Proc Natl Acad Sci USA* 105(48):18782–18787.
9. Thomas AG, et al. (2013) Kinetic characterization of ebselen, chelerythrine and apomorphine as glutaminase inhibitors. *Biochem Biophys Res Commun* 438(2):243–248.
10. DeLaBarre B, et al. (2011) Full-length human glutaminase in complex with an allosteric inhibitor. *Biochemistry* 50(50):10764–10770.
11. Thangavelu K, et al. (2012) Structural basis for the allosteric inhibitory mechanism of human kidney-type glutaminase (KGA) and its regulation by Raf-Mek-Erk signaling in cancer cell metabolism. *Proc Natl Acad Sci USA* 109(20):7705–7710.
12. Rahman A, Smith FP, Luc PT, Woolley PV (1985) Phase I study and clinical pharmacology of 6-diazo-5-oxo-L-norleucine (DON). *Invest New Drugs* 3(4):369–374.
13. Seltzer MJ, et al. (2010) Inhibition of glutaminase preferentially slows growth of glioma cells with mutant IDH1. *Cancer Res* 70(22):8981–8987.
14. Le A, et al. (2012) Glucose-independent glutamine metabolism via TCA cycling for proliferation and survival in B cells. *Cell Metab* 15(1):110–121.
15. Xiang Y, et al. (2015) Targeted inhibition of tumor-specific glutaminase diminishes cell-autonomous tumorigenesis. *J Clin Invest* 125(6):2293–2306.
16. Shukla K, et al. (2012) Design, synthesis, and pharmacological evaluation of bis-2-(5-phenylacetamido-1,2,4-thiadiazol-2-yl)ethyl sulfide 3 (BPTES) analogs as glutaminase inhibitors. *J Med Chem* 55(23):10551–10563.
17. Gross MI, et al. (2014) Antitumor activity of the glutaminase inhibitor CB-839 in triple-negative breast cancer. *Mol Cancer Ther* 13(4):890–901.
18. Harding JJ, et al. (2015) Safety and tolerability of increasing doses of CB-839, a first-in-class, orally administered small molecule inhibitor of glutaminase, in solid tumors. *J Clin Oncol* 33(15; Suppl):2512.
19. Xu Q, Boylan N, Hanes J (2012) Nanoparticles with enhanced mucosal penetration or decreased inflammation. US Patent Appl PCT/US2012/069882.
20. Yang Q, et al. (2014) Evading immune cell uptake and clearance requires PEG grafting at densities substantially exceeding the minimum for brush conformation. *Mol Pharm* 11(4):1250–1258.
21. Le A, et al. (2014) Tumorigenicity of hypoxic respiring cancer cells revealed by a hypoxia-cell cycle dual reporter. *Proc Natl Acad Sci USA* 111(34):12486–12491.
22. Xu Q, et al. (2013) Scalable method to produce biodegradable nanoparticles that rapidly penetrate human mucus. *J Control Release* 170(2):279–286.
23. Walters DM, et al. (2013) Clinical, molecular and genetic validation of a murine orthotopic xenograft model of pancreatic adenocarcinoma using fresh human specimens. *PLoS One* 8(10):e77065.
24. Dai L, Lu C, Yu XI, Dai LJ, Zhou JX (2015) Construction of orthotopic xenograft mouse models for human pancreatic cancer. *Exp Ther Med* 10(3):1033–1038.
25. Yabuuchi S, et al. (2013) Notch signaling pathway targeted therapy suppresses tumor progression and metastatic spread in pancreatic cancer. *Cancer Lett* 335(1):41–51.
26. Blackwood E, et al. (2013) Combination drug scheduling defines a "window of opportunity" for chemopotentiation of gemcitabine by an orally bioavailable, selective ChK1 inhibitor, GNE-900. *Mol Cancer Ther* 12(10):1968–1980.
27. Fan TW, et al. (2009) Altered regulation of metabolic pathways in human lung cancer discerned by (13)C stable isotope-resolved metabolomics (SIRM). *Mol Cancer* 8:41.
28. Fan TW, Lane AN, Higashi RM, Yan J (2011) Stable isotope resolved metabolomics of lung cancer in a SCID mouse model. *Metabolomics* 7(2):257–269.
29. Pelletier J, et al. (2012) Glycogen synthesis is induced in hypoxia by the hypoxia-inducible factor and promotes cancer cell survival. *Front Oncol* 2:18.
30. El-Mir MY, et al. (2000) Dimethylbiguanide inhibits cell respiration via an indirect effect targeted on the respiratory chain complex I. *J Biol Chem* 275(1):223–228.
31. Owen MR, Doran E, Halestrap AP (2000) Evidence that metformin exerts its anti-diabetic effects through inhibition of complex 1 of the mitochondrial respiratory chain. *Biochem J* 348(Pt 3):607–614.
32. Liu J, et al. (2013) Metformin inhibits renal cell carcinoma in vitro and in vivo xenograft. *Urol Oncol* 31(2):264–270.
33. Kisfalvi K, Moro A, Sinnett-Smith J, Eibl G, Rozengurt E (2013) Metformin inhibits the growth of human pancreatic cancer xenografts. *Pancreas* 42(5):781–785.
34. Avgoustakis K (2004) Pegylated poly(lactide) and poly(lactide-co-glycolide) nanoparticles: Preparation, properties and possible applications in drug delivery. *Curr Drug Deliv* 1(4):321–333.
35. Hrkach J, et al. (2012) Preclinical development and clinical translation of a PSMA-targeted docetaxel nanoparticle with a differentiated pharmacological profile. *Sci Transl Med* 4(128):128ra39.
36. Zimmermann SC, et al. (2016) Allosteric glutaminase inhibitors based on a 1,4-di(5-amino-1,3,4-thiadiazol-2-yl)butane scaffold. *ACS Med Chem Lett* 7(5):520–524.
37. Hu X, et al. (2009) Genetic alterations and oncogenic pathways associated with breast cancer subtypes. *Mol Cancer Res* 7(4):511–522.
38. Fan TWM, Tan J, McKinney MM, Lane AN (2012) Stable isotope resolved metabolomics analysis of ribonucleotide and RNA metabolism in human lung cancer cells. *Metabolomics* 8(3):517–527.
39. Le A, et al. (2010) Inhibition of lactate dehydrogenase A induces oxidative stress and inhibits tumor progression. *Proc Natl Acad Sci USA* 107(5):2037–2042.
40. Goodwin PJ, et al. (2015) Effect of metformin vs placebo on and metabolic factors in NCIC CTG MA.32. *J Natl Cancer Inst* 107(3):djv006.
41. Andrzejewski S, Gravel S-P, Pollak M, St-Pierre J (2014) Metformin directly acts on mitochondria to alter cellular bioenergetics. *Cancer Metab* 2:12.
42. Marchiq I, Le Floch R, Roux D, Simon MP, Pouyssegur J (2015) Genetic disruption of lactate/H^+ symporters (MCTs) and their subunit CD147/BASIGIN sensitizes glycolytic tumor cells to phenformin. *Cancer Res* 75(1):171–180.
43. Kisfalvi K, Eibl G, Sinnett-Smith J, Rozengurt E (2009) Metformin disrupts crosstalk between G protein-coupled receptor and insulin receptor signaling systems and inhibits pancreatic cancer growth. *Cancer Res* 69(16):6539–6545.
44. Cassago A, et al. (2012) Mitochondrial localization and structure-based phosphate activation mechanism of glutaminase C with implications for cancer metabolism. *Proc Natl Acad Sci USA* 109(4):1092–1097.
45. Guillaumond F, et al. (2013) Strengthened glycolysis under hypoxia supports tumor symbiosis and hexosamine biosynthesis in pancreatic adenocarcinoma. *Proc Natl Acad Sci USA* 110(10):3919–3924.
46. Rückert F, et al. (2012) Five primary human pancreatic adenocarcinoma cell lines established by the outgrowth method. *J Surg Res* 172(1):29–39.
47. Torres MP, et al. (2013) Novel pancreatic cancer cell lines derived from genetically engineered mouse models of spontaneous pancreatic adenocarcinoma: Applications in diagnosis and therapy. *PLoS One* 8(11):e80580.
48. Jones S, et al. (2008) Core signaling pathways in human pancreatic cancers revealed by global genomic analyses. *Science* 321(5897):1801–1806.
49. Feldmann G, et al. (2008) An orally bioavailable small-molecule inhibitor of Hedgehog signaling inhibits tumor initiation and metastasis in pancreatic cancer. *Mol Cancer Ther* 7(9):2725–2735.
50. Jimeno A, et al. (2009) A direct pancreatic cancer xenograft model as a platform for cancer stem cell therapeutic development. *Mol Cancer Ther* 8(2):310–314.
51. Rajeshkumar NV, et al. (2015) Therapeutic targeting of the Warburg effect in pancreatic cancer relies on an absence of p53 function. *Cancer Res* 75(16):3355–3364.
52. Lane AN, Fan TW, Higashi RM (2008) Isotopomer-based metabolomic analysis by NMR and mass spectrometry. *Methods Cell Biol* 84:541–588.
53. Fan TW, Lane AN (2011) NMR-based stable isotope resolved metabolomics in systems biochemistry. *J Biomol NMR* 49(3–4):267–280.
54. Lane AN, Fan TW-M, Xie Z, Moseley HN, Higashi RM (2009) Isotopomer analysis of lipid biosynthesis by high resolution mass spectrometry and NMR. *Anal Chim Acta* 651(2):201–208.
55. Moseley HN (2010) Correcting for the effects of natural abundance in stable isotope resolved metabolomics experiments involving ultra-high resolution mass spectrometry. *BMC Bioinformatics* 11:139.
56. Kanehisa M, et al. (2006) From genomics to chemical genomics: New developments in KEGG. *Nucleic Acids Res* 34(Database issue):D354–D357.
57. Joshi-Tope G, et al. (2005) Reactome: A knowledgebase of biological pathways. *Nucleic Acids Res* 33(Database issue):D428–D432.
58. Matthews L, et al. (2009) Reactome knowledgebase of human biological pathways and processes. *Nucleic Acids Res* 37(Database issue):D619–D622.
59. Romero P, et al. (2005) Computational prediction of human metabolic pathways from the complete human genome. *Genome Biol* 6(1):R2.
60. Wishart DS, et al. (2007) HMDB: The Human Metabolome Database. *Nucleic Acids Res* 35(Database issue):D521–D526.